Sensing and Bio-Sensing Research 45 (2024) 100579

Contents lists available at ScienceDirect

Sensing and Bio-Sensing Research

journal homepage: www.elsevier.com/locate/sbsr

Silicate-glass based photonic crystal fiber for rapid petro-chemical sensing: Design and analysis

Md Rezaul Hoque Khan [a,*], Md Sanowar Hosen [a,b], Atiqul Alam Chowdhury [a], Mohammad Rakibul Islam [a], Fahim Faisal [a], Mirza Muntasir Nishat [a], Nafiz Imtiaz Bin Hamid [a]

[a] Department of Electrical & Electronics Engineering, Islamic University of Technology, Dhaka, Bangladesh
[b] Department of Electrical & Electronics Engineering, Daffodil International University, Daffodil Smart City, Ashulia, Dhaka, Bangladesh

ARTICLE INFO

Keywords:
Optical sensor
Photonic crystal fiber
Relative sensitivity
Effective material loss
Analyte

ABSTRACT

The distillation method for extracting anhydrous ethanol from the volatile benzene water requires continuous supervision in the petro-chemical industry. This paper describes the design process and numerical analyses of a PCF sensor with a hollow core for sensing the petro-chemical constituents, namely ethanol, water, and benzene, in the 2 THz range. Photonic crystal fiber sensors have many possible applications in the petro-chemical industry, environmental monitoring, biomedicine, and food preservation. An optical fiber-based sensor with simultaneous low loss and enhanced sensitivity is intended to detect this petro-chemical effectively and safely. The Finite Element Method (FEM) framework is used to quantify the exhibition of the suggested fiber sensor. The simulation outcomes on the suggested sensor model demonstrate very satisfactory results on the relative sensitivity as 99.55 %, 99.44 % and 99.59 % confinement loss as 2×10^{-17} dB/cm, 1×10^{-16} dB/cm and 1.17×10^{-16} dB/cm, Effective Material Loss (EML) as 0.00043 cm^{-1}, 0.00054 cm^{-1} and 0.00038 cm^{-1} for Ethanol, Water and Benzene, respectively and the Effective areas (EAs) are 2.85×10^{-7} m^2 for Ethanol, 2.91×10^{-7} m^2 for Water and 2.82×10^{-7} m^2 for Benzene at 2 THz frequency regime.

1. Introduction

Distillation is a vital separation technique utilized in the petro-chemical sector that depends on the chemical properties of the constituent materials, specifically their differing boiling points or relative volatility, to effectively separate liquid mixtures [1]. In the petroleum industry, distillation is the most common and significant separation technique for final product purification. Each of the parts that make up a distillation column is employed to either improve mass transfer or transmit heat energy. A typical distillation column consists of a vertical column with trays or plates to help with component separation, a reboiler to provide heat for the necessary vaporization from the bottom of the column, a condenser to cool and condense the vapor from the top of the column, and a reflux drum to store the condensed vapor so that liquid reflux can be recycled back from the top of the column [2]. Most distillation control systems, whether traditional or modern, presumptively run the column at a constant pressure. Pressure changes impede performance and make control more challenging [3]. Conventional distillation columns generally cannot separate azeotropic mixtures or elements with boiling points that are very close (less than 20^0 C apart) in a single pass. In these situations, it is also used to alter the relative volatility of components that are approaching boiling or azeotropic formations by adding an extra component known as an entrainer, solvent, or mass-separating agent (MSA) [4]. In the petro-chemical sector, it is crucial to study how alcohol is distributed between the two practically immiscible solvents, water and benzene when they are combined with ethanol [5]. In the petro-chemical industry, the distillation mechanism for separating anhydrous ethanol from the benzene-water volatility [6], requires continuous monitoring, and traditionally such detection mostly relies on a laborious method [7].

Petro-chemicals can be monitored in the distillation process using a variety of techniques, including the experiment of density, the vaporization, and the vapor-liquid equilibrium (VLE) [8,9]. The methods mentioned above are lab-based, take a lot of time, and expensive raw materials and equipment. These methods are typically obliged by their affectability and precision. Very delicate, light, constrained, and intelligent fiber-based sensors will significantly advance the industry in these conditions. To address these challenges, there is a need for the

* Corresponding author.
E-mail address: rhkhan@iut-dhaka.edu (M.R.H. Khan).

https://doi.org/10.1016/j.sbsr.2023.100579
Received 9 May 2023; Received in revised form 27 July 2023; Accepted 7 August 2023
Available online 9 August 2023

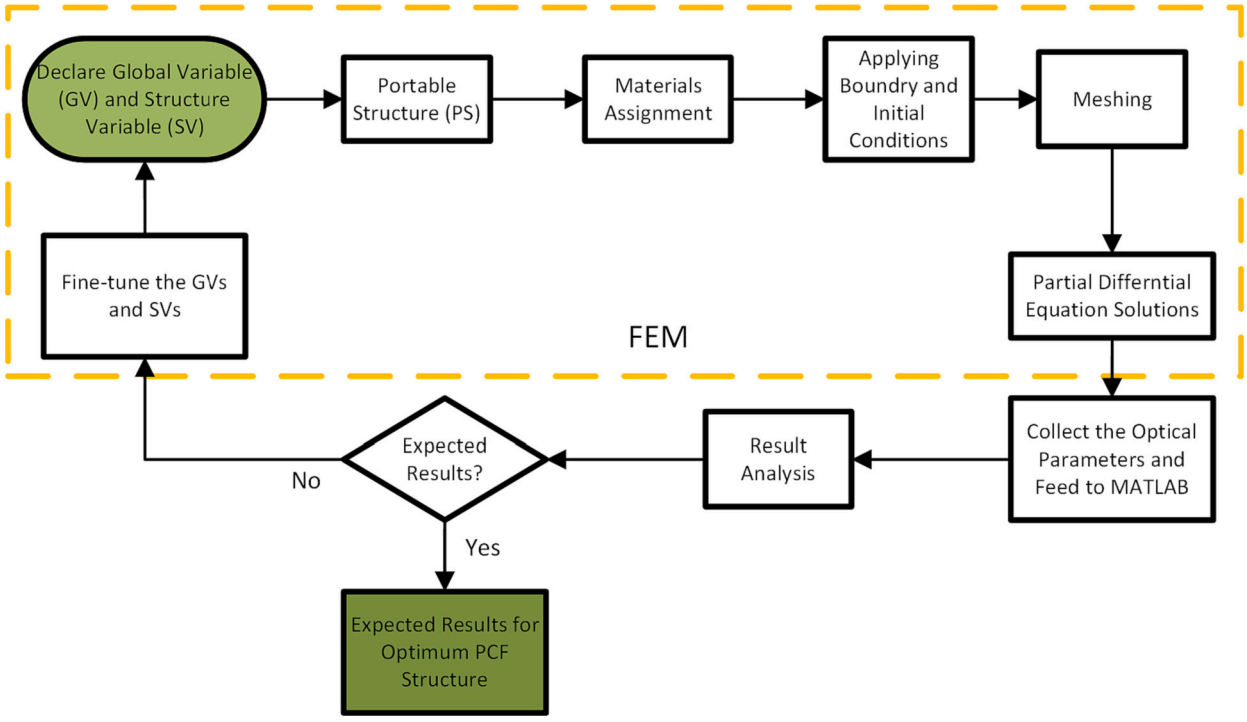

Fig. 1. The step-by-step process involved in designing and analyzing the model in this study.

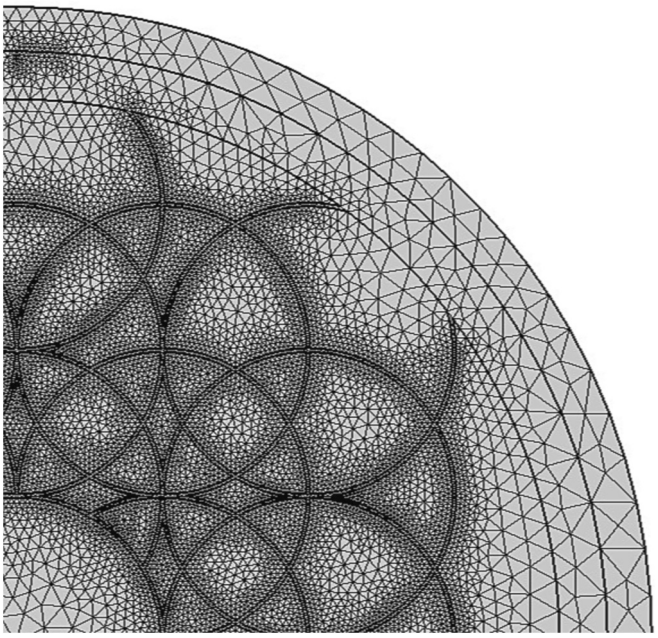

Fig. 2. Meshing output with boundary condition for A quarter segment of the Perfectly Match Layer (PML) layer computation window for the recommended PCF structure.

development of highly sensitive, compact, and cost-effective sensing solutions that can be integrated into the distillation process. Fiber-based sensors, such as fiber optic sensors, have gained attention as a promising technology for monitoring petro-chemicals during distillation [10]. These sensors rely on the interaction of light with the target substances, enabling real-time and continuous monitoring without the need for complex and expensive equipment. Fiber-based sensors offer several advantages in the petro-chemical industry. They can provide high sensitivity, rapid response times, and real-time monitoring capabilities

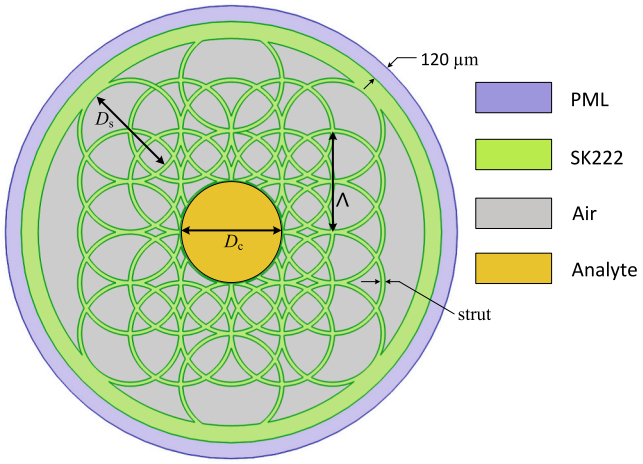

Fig. 3. Proposed rectangle core photonic crystal fiber.

[11]. Additionally, fiber sensors can be designed to be small, flexible, and immune to electromagnetic interference, making them suitable for use in harsh and hazardous environments. HC-PCF (Hollow-Core Photonic Crystal Fiber) is a type of optical fiber that has unique properties and has been explored as a sensing platform for petro-chemical analysis. Photonic Crystal Fiber (PCF) sensors are capable of meeting each need. There are various advantages to using PCF rather than conventional optical fibers, including the ability to employ extremely nonlinear and indefinitely single-mode large-mode fibers. Many optical properties, including polarization maintenance [12,13], propagation [14–16], low loss [13] and fiber birefringence [17] dynamically tuned with the help of purposeful cross-sectional patterning of the fiber. Hence, a variety of innovative fiber optic applications are feasible: Photonic crystal fiber-based high-power laser [18,19], tunable light switch [20] super continuum generation [21], dispersion compensation [22,23] fiber-optic sensors [19,24,25], interferometry [26,27], terahertz propagation [28]

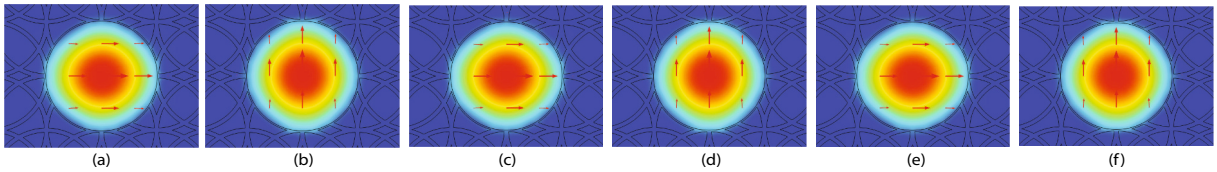

Fig. 4. Field distribution for different analytes inside the suggested HC-PCF's core. (a, b) Ethanol: x-pol & y-pol, (c, d) Water: x-pol & y-pol, (e, f) Benzene: x-pol & y-pol.

and refractometry [29,30].

The electromagnetic spectrum's microwave and infrared bands contain terahertz (THz) radiation, which has a frequency range of 0.1 to 10 THz. Terahertz (THz) radiation has been used for PCF in medical imaging [31,32], telecommunication [33], bio-photonics [34,35], environmental applications [36], pharmaceutical drug testing [37], and sensing applications [38–41].

In the Solid Core Photonic Crystal Fiber (SC-PCF), the core is made of robust silicon, while the cladding section is made up of several air rings. Possibly one of the most intriguing PCF types is the hollow core due to its distinct light-guiding characteristics. Hollow-Core PCF is a phrase used to describe a PCF with a number of small-sized silicate tubes running along its longitude and being optically guided by the hollow core (HC-PCF) [24]. While a hollow-core PCF structure was taken into consideration for our design, In comparison to the permeable core inside the core region the HC-PCF has higher analytical volumes, which improves the interaction of light and materials. A polarization mechanism is implemented by the HC-PCF as well. This has been proved by applying stress to the core [42,43] and by inducing birefringence due to a strong anisotropy in the hole's structure [44].

Several researchers have previously developed a number of geometrical Photonic Crystal Fibar (PCF) structures using liquid samples' THz spectrum for chemical sensing [45–49]. A number of geometrical design like heptagonal [50] octagonal [51,52], decagonal [53], hexagonal [54], elliptical [55], spiral cladding [56], honey comb cladding [57] etc. has already been suggested. At 1 THz, the article's sensitivity [52] detects Benzene and Ethanol at 77.14 % and 78.06%, respectively. Asaduzzaman et al. [58] has less than 50 % sensitivity elliptical core but a high birefringence is presented for Eethanol. For the purpose of detecting Benzene and Ethanol, a microstructured octangular PCF (O-PCF) sensor is available in Ademgil et al. [51]. A revised octagonal configuration of [51] in [59] demonstrates increased sensitivity levels of 87% and 47.35% for Ethanol and Benzene, respectively, while also exhibiting reduced confinement loss. According to the simulation results, [60] for water and the relative sensitivity of ethanol is greater, at 88 % or 91 %, respectively, quickly after 1.2 THz, with nearly minimal confinement loss. The PCF geometry's rectangular hollow core was created [47] and shows confinement loss is 1.71×10^{-14} dB/cm with the highest sensitivity of 94.4%. This study still prohibits certain crucial characteristics such as dispersion, NA (numerical aperture), and an effective field. As recently as 2021, a number of chemical and biosensors have been suggested within the terahertz regime [61–64]. A. Maidi et al. [63] and S. Sen et al. [61] both exhibit negligible relative sensitivity for ethanol, with values of 65.34 % and 78.56 % for Ethanol, respectively. Furthermore, features like Birefringence and EML (Effective material loss) are not noted in [61]. The low sensitivity is explained by a leaky Mode profile in [63]. The Hollow Core-Photonic Crystal Fiber bio-sensor developed by A. Habib et al. [62] is about 98% immensely sensitive with a low loss (< 0.025 dB/cm).

The petrochemical sample (ethanol, benzene, and water) is introduced into the central air hole of the HC-PCF, and a numerical study of the comprehensive sensitivity is carried out with the aid of a finite element method. (FEM). Alcohol liquid samples have been monitored using the designed PCF geometry, which, at 2 THz, has a sensitivity of more than 99 %. Additionally, a mathematical analysis of the many fundamental properties reveals extremely sensing capabilities, low loss, flattening dispersion, and low birefringence, which are superior to a number of earlier prototypes [61–64].

Although Zeonex, Teflon and Topas are utilized successfully in photonic fiber as background materials (PCF) [65–68], the sodium-calcium silicate glass SK222 (68.4% SiO_2, 12.3% Na_2O, 2.4% Al_2O_3, 2% B_2O_3, 0.7% K_2O) [69] was chosen as the background material for the concept. In this article, to further improve the sensitivity and other performances we propose a straightforward, extremely sensitive HC-PCF based on the background material of SK222. Due to their higher refractive index, PCFs formed of smooth glasses exhibit increased attenuation, making them desirable building blocks for new types of polymer- or liquid-infiltrated machinery like liquid crystals [70]. For the development of soft glass-based PCF production processes, SK222 is the appropriate test bed material because of its negligible cost and extremely superior rheological properties.

2. Numerical analysis

The proposed petro-chemical sensor has been designed and analyzed using the FEM which is the primary approach employed in this study. The steps involved in petro-chemical sensor design and performance evaluation are illustrated in Fig. 1. Initially, the Global variables (GVs) and Structure variables (SVs) were declared in COMSOL Multiphysics 5.5 software, followed by the design of the PCF sensor structure. Materials were then assigned to different parts of the sensor, including SK222 to PML (Perfectly Match layer) and Strut of the fiber sensor, air-holes in the cladding, and analyte in the core for analysis purposes. Boundary and initial conditions were applied, and the designed fiber was meshed and solved using partial differential equations. The optical parameter data was then collected and transferred to MATLAB for further analysis. Different results were analyzed, and the relationship be-tween the operating frequency and various optical parameters was observed. If the results were not satisfactory, the GVs and SVs were adjusted, and the entire process was repeated until the desired results were achieved [71].

A list of different optical properties, such as relative sensitivity, effective area, numerical aperture(NA), CL (Confinement loss), EML, etc., seems necessary to check the petrochemical sensor's functionality. These parameters, i.e. performance indices, will be investigated through simulation using the software while injecting an analyte into the core of the proposed sensor using a capillary injection strategy. In actuality, though, this function will be fulfilled by an optical spectrum analyzer. For each analyte, the full procedure will be repeated.

For numerically resolving issues, the FEM with a Perfectly Match Layer (PML) boundary condition is frequently utilized. For investigating optical properties and removing leaks, a PML is utilized. A meshing technique is used to partition the proposed PCF into homogeneous triangular sub-spaces. Modal analysis and frequency transmission through the Z-direction of fiber can be used to determine the performance of waveforms spanning $1.5 - 3$ THz in an x-y cross-section. The following equation can be obtained using the Maxwell equations: [72].

$$\Delta \times [s]^{-1} \times E - k_0^2 n^2 [s] E = 0 \tag{1}$$

Where,

$s =$ Perfectly Match Layer (PML) matrix of 3×3, $[]^{-1} =$ is the inverse

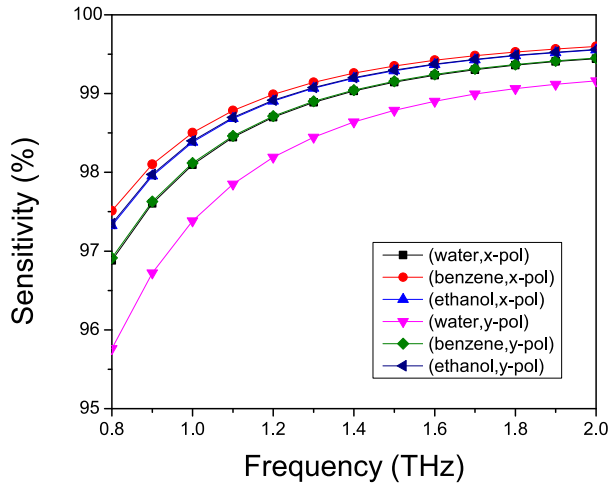

(a) $S = 10\ \mu m$

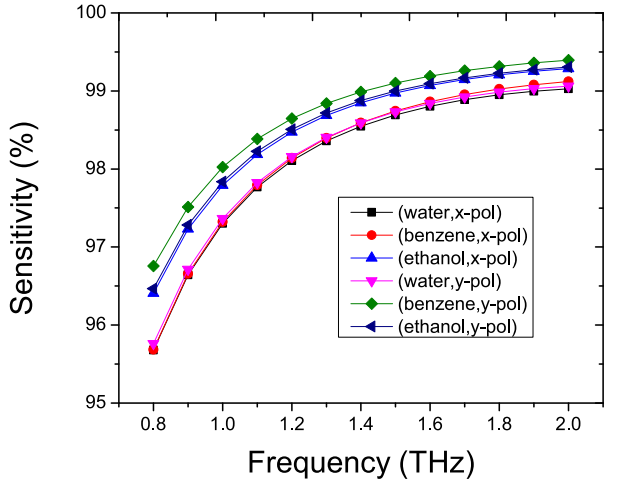

(b) $S = 20\ \mu m$

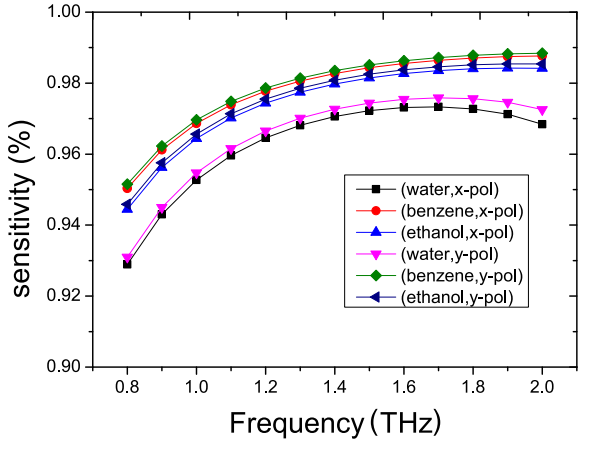

(c) $S = 30\ \mu m$

Fig. 5. Frequency dependent relative sensitivity of water, ethanol for (a) S=10 μm (b) S=20 μm (c)S=30 μm.

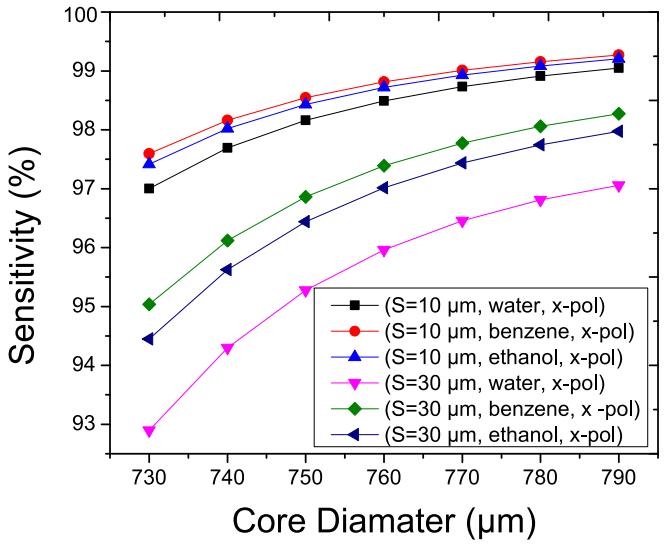

Fig. 6. Relation between the relative sensitivity and core diameter for Ethanol, Water and Benzene for strut width S = 10 μm, S = 20 μm and S = 30 μm.

Table 1
The suggested HC-PCF's geometrical variables that have been optimized.

	Core diameter, D_c **(**μm**)**	**Strut,** S **(**μm**)**
Optimum	**790**	**10**
	790	20
	790	30

of s,

E = Electric field vector,
n = domain refractive index,
K_0 = free-space wave number,
λ = operational wavelength,
E = is the field vector,

In this simulation, the fiber is split into 2,923,972 triangular segments. One-fourth of the PML layer computation window is used to display Fig. 2 for the recommended PCF structure.

The effectiveness of detecting chemicals in a terahertz PCF relies solely on how strong the interaction is between matter and light. Depending on a specific frequency absorption coefficient is necessary. This can be explained by the Beer-Lambert law [72]. The Beer-Lambert law is commonly applied to chemical analysis measurements to determine the concentration of chemical species that absorb light. It is often referred to as Beer's law and expressed by this equation,

$$I(f) = I_0(f)e^{[-r\alpha_m l_c]} \tag{2}$$

Where,
$I_0(f)$ = optical intensity in the absence of the intended substance,
$I(f)$ = optical intensity in the presence of the intended substance,
f = the optical frequency,
α_m = absorption factor,
r = the relative sensitivity,
l_c = the channel range,

The light absorbance (A) is proportional to concentration and can be explained as

$$A = log\frac{I}{I_0} = -r\alpha_m l_c \tag{3}$$

Now, the sensitivity must be determined in order to analyze the PCF's sensing effectiveness, which can be done using [44],

$$r = \frac{n_r}{n_{\text{eff}}} \times Y \tag{4}$$

Table 2
The optical properties of the suggested HC-PCF sensor for petrochemical sensing at 2.0 THz.

Analyte	RS (%)	CL (dB/cm)	EML (cm^{-1})	EA (m^2)	B	β	NA
Ethanol	99.55	2×10^{-17}	0.00043	2.85×10^{-7}	0.0000021	0.07962	0.15481
Water	99.43	1×10^{-16}	0.00054	2.91×10^{-7}	0.0000033	0.07962	0.15481
Benzene	99.59	1.17×10^{-16}	0.00038	2.82×10^{-7}	0.0000016	0.07962	0.15481

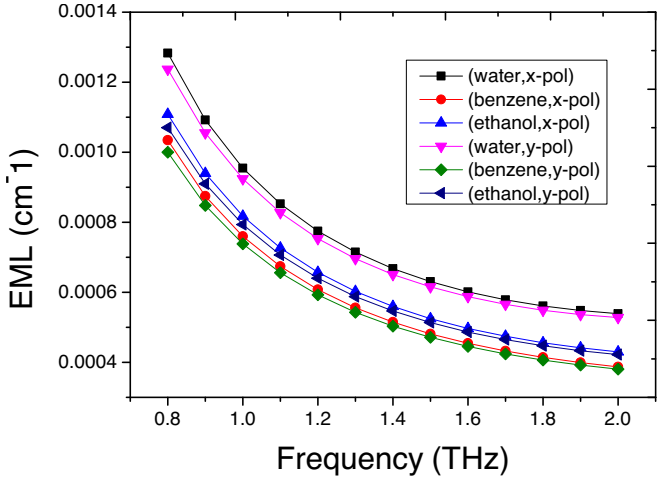

Fig. 7. The relation between EML and frequency for Ethanol, Water, and Benzene.

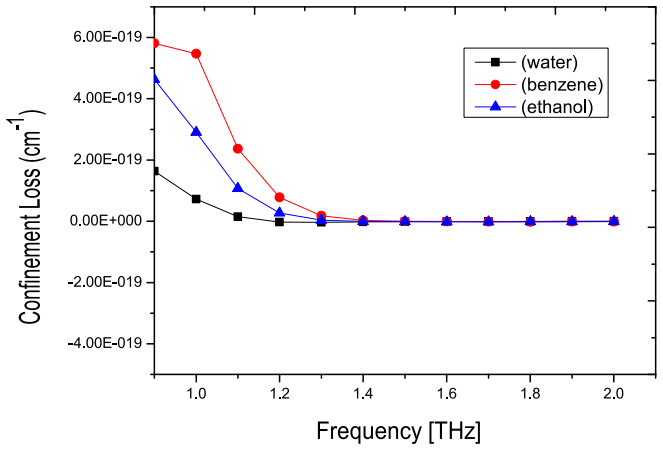

Fig. 8. The relation between confinement loss and frequency for Ethanol, Water and Benzene.

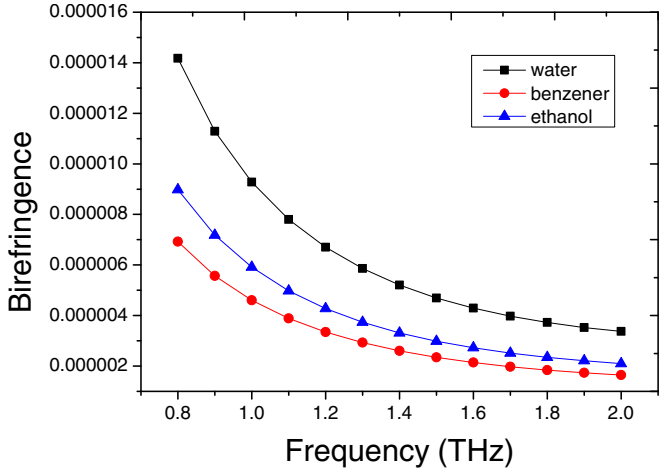

Fig. 9. The relation between birefringence and frequency for Ethanol, Water, and Benzene.

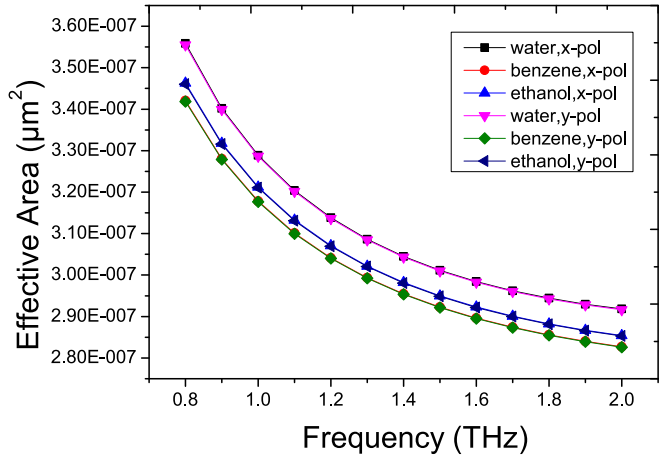

Fig. 10. The frequency dependent effective area for Ethanol, Water and Benzene for x polarization.

where,

n_r = the refractive index (RI) (real) of the analyte to be detected,

n_{eff} = the Effective RI (ERI) of the guided mode,

Y = represents the light interactivity with substance,

Which is determined by [44,73].

$$Y = \frac{\int_{\text{analytesample}} R_e\left(E_x H_y - E_y H_x\right) dxdy}{\int_{\text{total}} R_e\left(E_x H_y - E_y H_x\right) dxdy} \tag{5}$$

In this case,

E_x = the electric field components of x,

E_y = the magnetic field components of y,

The PCF should be the only source of light in the core area. Any optical power that crosses to the cladding air slot as a result of optical power escaping is treated as light power loss that occurs during confinement loss and is Stated as

$$\alpha(dB/cm) = 8.686 \times k_o Im\left[n_{\text{eff}}\right] \times 10^4 \tag{6}$$

where,

$Im\left[n_{\text{eff}}\right]$ = the imaginary segment of the effective mode index,

During the spreading of light pulses across the fiber, the guided mode experiences certain unintended losses. These properties of the PCFs are examined using EML, α_{eff}, which is be quantified as

$$\alpha_{\text{eff}} = \frac{1}{2}\sqrt{\frac{\varepsilon_0}{\mu_0}}\left(\frac{\int |E|^2 \alpha_{\text{m}} \eta \, dA}{2\int_{\text{All}} S_z dA}\right) \tag{7}$$

Where,as background material SK222,

α_{mat} = represents the loss of absorption,

n_{m} = the refractive index (RI),

ε_0 = the permittivity of free space,

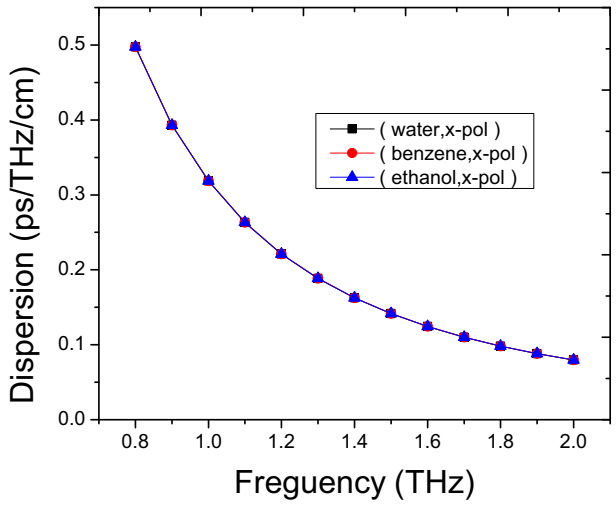

Fig. 11. Frequency corresponding dispersion for Ethanol, Water and Benzene for x polarization.

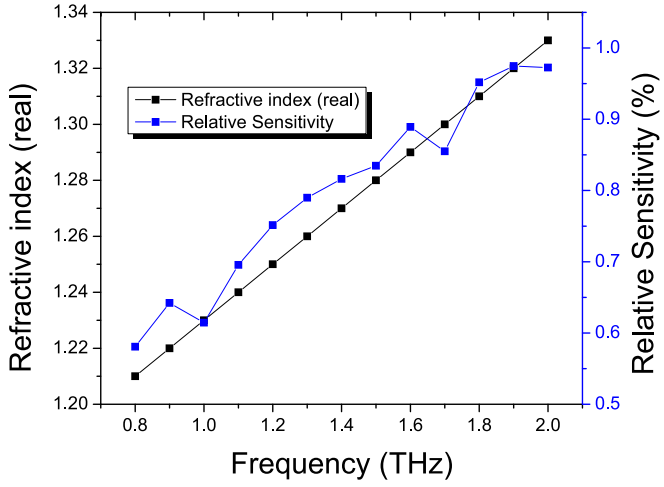

Fig. 12. Simultaneous illustration of relative sensitivity and ERI as in relation of frequency for Ethanol.

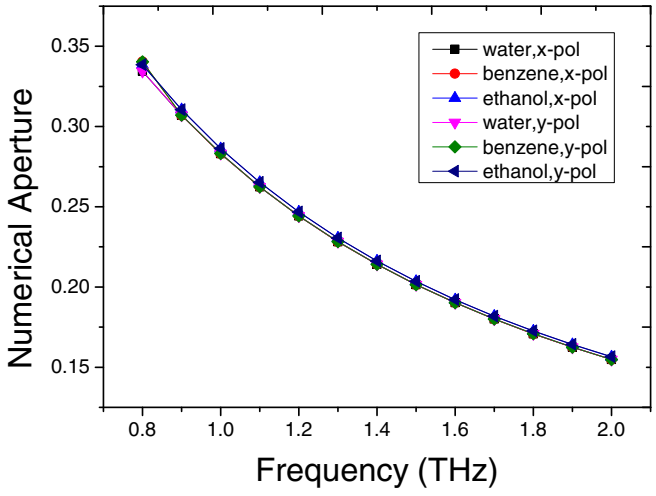

Fig. 13. Numerical aperture for Water, Benzene and Ethanol as a function of frequency.

μ_0 = represents the permeability into free space,
S_z = the z-component of the Poynting vector,

The physical phenomenon known as birefringence occurs when a substance's refractive index is determined by the direction or polarization of the distribution of light. The material's apparent birefringence will be broken by the fiber's cylindrical symmetry, and it may also acquire birefringence, resulting in regular power exchanges between the two components. The mathematical representation of birefringence is as follows:

$$B = |n_x - n_y| \tag{8}$$

where n_x and n_y are the refractive indexes of fiber in axial and transverse direction respectively.

In the analysis of the suggested THz PCF attributes, Another important element is the effective area. Effective area is the area that is covered by the light as it is traveling through the PCF. It depends on the wavelength, shape of the PCF and effective refractive index. It was initially developed as a measure of non-linearity; a low effective area indicates a high power density necessary for non-linear effects to be meaningful. It is important for the loss of confinement, loss of bending, and the numerical aperture. This property also serves to illustrate the light beams' efficiency. The mathematical representation of the effective area [74], A_{eff} is Stated as:

$$A_{\text{eff}} = \frac{\left(\iint_S |E|^2 dxdy\right)^2}{\iint_S |E|^4 dxdy} \tag{9}$$

where S refers to the entire cross-segment of the fiber and E is the field vector.

Another crucial aspect for multi-channel connection applications to be reduced is dispersion. Point to be noted that for the whole spectrum of $0.8 - 2$ THz, it was determined that the material dispersion for the PCF for SK222 was minimal. The only factor taken into account is the waveguide dispersion. The waveguide's ERI variance is the only factor that determines the dispersion of the waveguide. The following equation can be used to calculate it [72],

$$\beta_2 = \frac{2}{c}\frac{dn_{\text{eff}}}{dw} + \frac{w}{c}\frac{d^2 n_{\text{eff}}}{dw^2} \tag{10}$$

where, w represents the angular frequency and c represents the free space propagation velocity, respectively.

The numerical aperture (NA) calculates a PCF core's capability for light aggregation. Hence, the variation of the index of refraction can be calculated as follows [44].

$$NA = \frac{1}{\sqrt{\left(1 + \frac{\pi f^2 A_{\text{eff}}}{c^2}\right)}} \tag{11}$$

where, A_{eff} represents the effective area in the guided mode.

3. Detail design of the proposed HC-PCF

A hollow core PCF has a much bigger volume in the core area, which has a significant potential to boost sensitivity. Additionally, hollow core significantly minimizes the amount of background material used during manufacture, which in turn reduces material loss absorption. The whole intersection of the suggested HC-PCF is shown in Fig. 3. This article use the FEM [71,75,76] as a computational tool to investigate mode propagation characteristics. The simulations were performed using the COMSOL Multiphysics 5.5 software.

The term pitch distance, $\wedge$ refers to the distance between two adjacent cladding air-holes. The cladding air-holes have a diameter D_s. The Diameter of the core air-holes is designated as D_c. The suggested PCF's

Table 3
Table comparing the HC-PCF fiber we recommended to the previously described PCF.

Ref.	Analyte	Frequency/wavelength	RS (%)	CL (dB/cm)	EML (cm^{-1})	EA (m^2)	B
[52]	Ethanol	1 THz	77.14	2.26×10^{-06}	–	1.46×10^{-7}	–
[77]	Ethanol	1.4 THz	96:8	6.95×10^{-14}	0.0035	–	0.0154
[78]	Ethanol	1.5 μm	23.75	5.5×10^{-05}	–	–	–
[79]	Ethanol	1.33 μm	67.66	7.5×10^{-12}	–	–	–
[50]	Ethanol	1 THz	68.48	5.2×10^{-8}	–	1.644×10^{-07}	–
[58]	Ethanol	1.33 μm	48	8.1×10^{-12}	–	–	0.001544
[59]	Ethanol	1.33 μm	46.31	2.28217×10^{-14}	–	–	–
[61]	Ethanol	1 THz	78.56	6.02×10^{-8}	–	1.4×10^{-7}	–
[63]	Ethanol	1.3 μm	65.34	1×10^{-8}	–	1.965	0.0015
[80]	Water	1.5 THz	79.39	4.93×10^{-12}	–	1.66×10^{-7}	–
[81]	Water	1.6 THz	60.03	1×10^{-11}	–	1.63×10^{-8}	–
[61]	Water	1 THz	77.51	5.74×10^{-8}	–	1.45×10^{-10}	–
[82]	Water	1.8 THz	74.54	7.72×10^{-8}	0.0168	–	–
[83]	Water	1 THz	85.6	4.5×10^{-9}	–	7.11×10^{-8}	–
[84]	Water	1.7 THz	92.9	1.61×10^{-13}	0.0054	7.11×10^{-7}	–
[80]	Benzene	1.5 THz	80.27	1.33×10^{-12}	–	1.49×10^{-7}	–
[81]	Benzene	1.6 THz	63.24	1.2×10^{-11}	–	1.44×10^{-7}	–
[61]	Benzene	1 THz	79.76	6.02×10^{-8}	–	1.35×10^{-10}	–
[82]	Benzene	1.8 THz	74.91	4.51×10^{-10}	0.0135	–	–
[83]	Benzene	1 THz	85.9	1.02×10^{-9}	–	6.93×10^{-8}	–
[84]	Benzene	1.7 THz	94.2	1.28×10^{-13}	0.0059	3.13×10^{-7}	–
Proposed HC-PCF	Ethanol	2 THz	99.55	2×10^{-17}	0.00043	2.85×10^{-7}	0.0000021
Proposed HC-PCF	Water	2 THz	99.43	1×10^{-16}	0.00054	2.91×10^{-7}	0.0000033
Proposed HC-PCF	Benzene	2 THz	99.59	1.17×10^{-16}	0.00038	2.82×10^{-7}	0.0000016

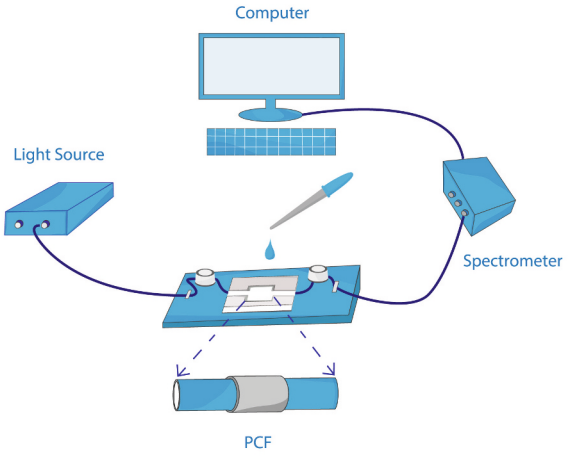

Fig. 14. Schematic Diagram of this work for petro-chemical Detection.

structural parameters are $\wedge = 770\ \mu m$, $D_s = 740\ \mu m$ and $D_c = 790\ \mu m$. The term "strut" refers to the air-hole cladding thickness. A desirable strut thickness is maintained throughout the procedure to avoid manufacturing challenges. While a range of strut widths, S, of 10 μm, 20 μm and 30 μm is taken into consideration, contemporary manufacturing techniques can handle strut widths of 6.5 μm. The perfectly matched layer has a thickness of 120 μm and a diameter of 1600 μm. Any modification to the cladding's shape or size may impact confinement loss, but it has no impact whatsoever on the core analyte.

As an anti-reflective layer, a perfectly matched layer (PML) is put in place at the cladding's edge [44] in order to absorb the incoming PCF waves. The width of PML matters since it has a great impact on numerical analysis. Convergence tests were conducted as a consequence, and it was discovered that the best results were obtained at a thickness of PML over 10% of the whole diameter. It should be noted that other petro-chemical analytes, such as ethanol, water, and benzene, were utilized instead of air in the hollow central sections. These analytes had respective indexes of refraction of 1.354, 1.33, and 1.366 [68].

4. Simulation results and discussions

Fig. 4 shows the optical field strength when a petrochemical sample (i.e., ethanol, benzene, water) is present. The optical field's polarizations (x-pol and y-pol) are shown to have very well-guided modes.

Fig. 5 illustrates the relationship between the relative sensitivity and corresponding frequency of three different strut widths of 10 μm, 20 μm and 30 μm for the core diameter D_c=790 μm for ethanol, water, and benzene.

Figures clearly show that all three analytes would have better sensitivity with a narrower strut. It has also been demonstrated that relative sensitivity increases up to a particular frequency before essentially flattening off. This is expressed as follows: when the frequency rises, the core power percentage rises as well, improving the effective RI. As from Equ. (4) The analyte's RI and the effective RI may be demonstrated to directly and inversely correspond, respectively, to the relative sensitivity.

Fig. 6 depicts the relationship between the relative sensitivity for different core diameters for ethanol. In this instance, a plot for the sensitivity is realized by altering the core size. The sensitivity is plotted for the strut with S = 10 μm, S = 20 μm and S = 30 μm.

The optimal value, which will be used throughout the manuscript, was found with a core diameter of D_c=790 μm and a strut with S=10 μm. Relative sensitivity is seen to rise when the core dimension does as well. For the suggested HC-PCF design, the recommended scale D_c=790 μm and S=10 μm is the highest and will surpass the cladding area if additional advancements are made.

Where as the core power fraction achieved in this mode is larger than that of y-polarization, x-polarization has a higher relative sensitivity of the y-polarization.

The suggested HC-PCF's optimized geometrical variables, which were obtained from Fig. 5 and Fig. 6, are compiled in Table 1 and that will be utilized to examine different performance characteristics throughout the manuscript. (See Table 2.)

The effective analyte detection of a Terahertz sensor is constrained by a small number of limiting parameters, including the EML and CL and bending and scattering losses.

Please take note that Fig. 4 expressly states that the interaction of light with the cladding is low and strictly controlled the light in the core,

ignoring the scattering loss feature. Furthermore, it is better to avoid characterizing the bending loss due to the length consideration. Therefore, by including air spaces in the core region, the EML(which develops as a result of the background material used, and may be reduced) is the main contributor to optical power loss in the proposed PCF. Another benefit of employing a hollow core is that it may significantly reduce the thickness of background material from the core, which reduces EML.

Fig. 7 shows EML characteristics in relation to the frequency of changes in analytes. As shown, EML reduces in response to the frequency at optimal geometrical variables, ultimately fulfilling the theoretical state of the EML computation [58,77]. Additionally, Fig. 7 demonstrates that the EML is as small as 0.00043 cm^{-1}, 0.00054 cm^{-1} and 0.00038 cm^{-1} for Ethanol, Water and Benzene, respectively.

Fig. 8 demonstrates the relationship between the frequency of different analytes and confinement loss.

As the frequency rises, the confinement loss decreases for all three analytes because the hollow core area's mode fields constrict more tightly. As a consequence, ethanol confinement loss decreases by 2×10^{-17} dB/cm, water confinement loss decreases by 1×10^{-16} dB/cm, and benzene confinement loss decreases by 1.17×10^{-16} dB/cm.

The acquired EMLs are quite unimportant in comparison to the obtained EML.

In Fig. 9, the birefringence property is seen by the analytes. As the frequency ultimately increases in x-polarity and y-polarity, the birefringence descends with decreasing ERI. The analytes can see the birefringence characteristic in Fig. 9. In both x-polarization and y-polarization, the ERI steadily decreases for each analyte as the frequency increases due to the birefringence decreasing. At optimal circumstances, the obtained birefringence for ethanol, water, and benzene as 0.0000021, 0.0000033 and 0.0000016, respectively. Please be aware that theoretically, reducing the core size might raise the birefringence even more, but this would significantly reduce the relative sensitivity.

The frequency dependency of the effective area for several analytes is shown in Fig. 10. The visual representations of this figure show that the effective mode area decreases with increasing frequency. At higher frequencies in the core portion, the mode field is highly confined, and the effective area is less. At ideal design conditions, the suggested PCF exhibited a moderate effective area value for ethanol of 2.85×10^{-7} m^2. Fig. 8 illustrates this physical result, demonstrating how confinement loss diminishes as frequency rises.

The frequency dependent dispersion relation for each analyte applied to the suggested PCF is shown in Fig. 11. As can be seen, the dispersion decreases as the frequency increases.

In Fig. 12,shows a simultaneous plot of the relative sensitivity and the ERI (real) in response to frequency for ethanol. As can be shown, the adaption of the cladding air hole's size scarcely has an impact on the PCF's sensing capability. On the other hand, larger dimensions increase the cladding size, which results in stronger optical signal confinement because of reduced confinement loss. Although, this enlarges the sensor and gives it more mass. Therefore, depending on the size and fabrication tolerance of the PCF as indicated in Section 3, we choose the best dimension.

Fig. 13 shows the numerical aperture for Benzene, Water, and Ethanol in relation to frequency. The graph depicts how NA behaves, acting downward with gradually increasing frequency. In contrast to the original set point of 2.2 THz frequency, which was intended to provide optimal performance, an increased NA of 0.34 is obtained at the 1 THz frequency mark.

Table 3 compares the suggested PCF model to previously reported PCF based on a variety of performance criteria and outperforms the earlier design in terms of sensitivity.

5. Fabrication of the suggested HC-PCF

Another significant issue is the manufacture of PCF-based devices. In spite of the development of numerous manufacturing techniques, including boiling techniques, capillary packing, multiple thinning, casting, and the sol-gel and stacking and drawing method [85–93] – all of which have been used to create hollow-shaped processes – 3D printing was utilized for creating a number of hollow-shaped core processes [92]. Several PCF structures have been created by D. Pysz et al. using the stack and draw technique [91]. Additionally, Z. Lui et al. [94] presented various stack and draw techniques for fabricating suspended microstructure fibers. Recently, it was reported that a hollow core PCF was developed using the stack-and-draw method, which involves stacking several layers of extruded material on top of each other and then drawing the whole structure into its final shape and was based on sodium-calcium-silicate glass [95]. The HC-PCF-based sensor can be rendered using normal stack-and-drawing technology and includes circle-formed air holes both in the center and cladding [96,97]. By leaving out some capillaries, it is possible to create a hollow air core and claddings. In light of current fabrication methods and their shortcomings, we proposed an HC-PCF petro-chemical sensor that could be produced in any extrusion or 3D printing manufacturing environment.

Fig. 14 shows the basic structure for detecting petro-chemical using the proposed sensor. In the figure, light is incident upon the core of the biosensor which is filled with analyte. The light passes through the analyte in the biosensor and goes into the spectrometer. Spectrometer is used to analyze spectral properties of the fiber which can provide information about the refractive index of the surrounding medium and any analytes present. Spectrometer can also be used to monitor changes in the transmission spectra of the fiber over time, which can be used for real-time sensing applications. All these data is transferred to a PC for further analysis and comparison.

6. Application possibilities of the proposed HC-PCF

The sensor was demonstrated to have extremely high sensitivity (supposedly surpassing 99%) for analytes with a 1.3–1.4 RI range while operating at peak efficiency. The suggested sensor could be used as a biosensor for blood component detection in the medical field [98]. Red blood cells have a RI of 1.40, while hemoglobin has a RI of 1.38, white blood cells have a RI of 1.36, plasma has a RI of 1.35, and water has a RI of 1.33 [34]. Moreover, the suggested sensor can differentiate between different types of alcohol (i.e. Ethanol, Benzene, Methanol) [72]. So, it is evident that the suggested sensor can identify cancer cells and other substances in a variety of industries. Moreover, given the large detecting range, it is evident that the proposed sensor model may detect biochemicals or other compounds in a variety of sectors.

7. Conclusions

The design and numerical inquiry for evaluating the sensing performance of a hollow-core PCF at 2 THz for the three widely-known elementary chemical constituents, namely water, ethanol, and benzene, are done in this research. After doing the entire experiment, we discovered that the same analytes had substantially higher sensitivity for ethanol, water, and benzene, measuring 99.55 %, 99.43 % and 99.59 % respectively, along with incredibly small confinement losses of 2×10^{-17} dB/cm, 1×10^{-16} dB/cm and 1.17×10^{-16} dB/cm and EML as 0.00043 cm^{-1}, 0.00054 cm^{-1} and 0.00038 cm^{-1} for Ethanol, Water and Benzene, respectively. The EAs are 2.85×10^{-7} m^2 for Ethanol, 2.91×10^{-7} m^2 for Water and 2.82×10^{-7} m^2 for Benzene. Additionally, numerical aperture measurements are performed in this inquiry, with a favorable outcome. The proposed petrochemical sensor holds significant potential for future implementation and can be enhanced by incorporating additional bio applications such as Microfluidic Invasion Chemotaxis Platform for 3D Neurovascular Co-Culture [99] and 3D-Printed Microneedles (MNs) [100]. Furthermore, the implementation of 3D-Printed MNs offers numerous advantages, such as user-

friendliness, minimal invasiveness, reduced pain, and lower tissue damage compared to conventional needles. These microneedles can be utilized for the collection of analytes from the human body, serving as a convenient and efficient interface between the sensor and the target sample. The integration of 3D-Printed MNs enhances the usability and acceptance of the sensor, making it more accessible and suitable for various applications. The proposed petrochemical sensor exhibits improved sensitivity and features sophisticated packaging to protect the detecting head. This ensures accurate and reliable detection of different petrochemicals. Additionally, recent advancements in 3D nano-fabrication methods provide a promising avenue for the realization of the suggested Photonic Crystal Fiber (PCF) structures, further supporting the practical implementation of the sensor [71,101,102]. This simulated observation also yields a greater effective area with a minimal EML and propagation constant. As a result, we may draw the conclusion that the suggested sensor has the potential to be used to any type of chemical in the petrochemical sector.

Funding

The funding for this research was provided by the Islamic University of Technology, located in Dhaka, Gazipur 1704, Bangladesh, under the title"IUT Seed Grant." The grant number for this project is REASP/IUT-RSG/2022/OL/07/009.

Author statement

We declare that this manuscript is original, has not been published before and is not currently being considered for publication elsewhere.

We confirm that the manuscript has been read and approved by all named authors and that there are no other persons who satisfied the criteria for authorship but are not listed. We further confirm that the order of authors listed in the manuscript has been approved by all of us.

We understand that the Corresponding Author is the sole contact for the Editorial process. He is responsible for communicating with the other authors about progress, submissions of revisions and final approval of proofs.

Declaration of Competing Interest

None.

Data availability

Data will be made available on request.

References

[1] E. Rocha, M. Lopes, M. Maciel, R. Filho, L. Medina, Recovery and characterization of petroleum residues through the molecular distillation process, Pet. Sci. Technol. 32 (20) (2014) 2450–2457.
[2] H. Devold, Oil and gas production handbook: an introduction to oil and gas production, Lulu. com, 2013.
[3] V.T. Minh, Modeling and control of distillation column in a petroleum process, in: 2010 5th IEEE Conference on Industrial Electronics and Applications, IEEE, 2010, pp. 259–263.
[4] Z. Lei, C. Li, B. Chen, Extractive distillation: a review, Sep. Purif. Rev. 32 (2) (2003) 121–213.
[5] J.J. Gutiérrez-Sevillano, S. Calero, R. Krishna, Separation of benzene from mixtures with water, methanol, ethanol, and acetone: highlighting hydrogen bonding and molecular clustering influences in cubtc, Phys. Chem. Chem. Phys. 17 (2015) 20114–20124, https://doi.org/10.1039/C5CP02726H.
[6] I. Gil, A. Uyazán, J. Aguilar, G. Rodírguez, L. Caicedo, Separation of ethanol and water by extractive distillation with salt and solvent as entrainer: process simulation, Braz. J. Chem. Eng. 25 (1) (2008) 207–215.
[7] W.-C. Shen, I.-L. Chien, Design and control of ethanol/benzene separation by energy-saving extraction–distillation process using glycerol as an effective heavy solvent, Ind. Eng. Chem. Res. 58 (31) (2019) 14295–14311.
[8] M. De, A.K. Pathak, V.K. Singh, Single channel photonic crystal fiber based high sensitive petrol adulteration detection sensor, Optik 183 (2019) 539–546.
[9] E. Haaz, D. Fozer, A.J. Toth, Development of anhydrous ethanol purification: reduction of acetal content and vapor–liquid equilibrium study of the ethanol–acetal binary system, ACS Omega 6 (2) (2021) 1289–1298.
[10] R.K. Gangwar, S. Kumari, A.K. Pathak, S.D. Gutlapalli, M.C. Meena, Optical fiber based temperature sensors: a review, Optics 4 (1) (2023) 171–197.
[11] X.-D. Wang, O.S. Wolfbeis, Fiber-optic chemical sensors and biosensors (2013–2015), Anal. Chem. 88 (1) (2016) 203–227.
[12] H. Kubota, S. Kawanishi, S. Koyanagi, M. Tanaka, S. Yamaguchi, Absolutely single polarization photonic crystal fiber, IEEE Photon. Technol. Lett. 16 (1) (2004) 182–184.
[13] K. Suzuki, H. Kubota, S. Kawanishi, M. Tanaka, M. Fujita, Optical properties of a low-loss polarization-maintaining photonic crystal fiber, Opt. Express 9 (13) (2001) 676–680.
[14] J.-S. Chiang, T.-L. Wu, Analysis of propagation characteristics for an octagonal photonic crystal fiber (o-pcf), Opt. Commun. 258 (2) (2006) 170–176.
[15] T.A. Birks, J.C. Knight, P.S.J. Russell, Endlessly single-mode photonic crystal fiber, Opt. Lett. 22 (13) (1997) 961–963.
[16] H. Han, H. Park, M. Cho, J. Kim, Terahertz pulse propagation in a plastic photonic crystal fiber, Appl. Phys. Lett. 80 (15) (2002) 2634–2636.
[17] Y.-S. Sun, Y.-F. Chau, H.-H. Yeh, D.P. Tsai, Highly birefringent index-guiding photonic crystal fiber with squeezed differently sized air-holes in cladding, Jpn. J. Appl. Phys. 47 (5R) (2008) 3755.
[18] D.J. Richardson, J. Nilsson, W.A. Clarkson, High power fiber lasers: current status and future perspectives, JOSA B 27 (11) (2010) B63–B92.
[19] J. Limpert, N. Deguil-Robin, I. Manek-Hönninger, F. Salin, F. Röser, A. Liem, T. Schreiber, S. Nolte, H. Zellmer, A. Tünnermann, et al., High-power rod-type photonic crystal fiber laser, Opt. Express 13 (4) (2005) 1055–1058.
[20] F. Du, Y.-Q. Lu, S.-T. Wu, Electrically tunable liquid-crystal photonic crystal fiber, Appl. Phys. Lett. 85 (12) (2004) 2181–2183.
[21] S. Coen, A.H.L. Chau, R. Leonhardt, J.D. Harvey, J.C. Knight, W.J. Wadsworth, P. S.J. Russell, Supercontinuum generation by stimulated raman scattering and parametric four-wave mixing in photonic crystal fibers, JOSA B 19 (4) (2002) 753–764.
[22] L. Shen, W.-P. Huang, G. Chen, S. Jian, Design and optimization of photonic crystal fibers for broad-band dispersion compensation, IEEE Photon. Technol. Lett. 15 (4) (2003) 540–542.
[23] F. Poli, A. Cucinotta, S. Selleri, A. Bouk, Tailoring of flattened dispersion in highly nonlinear photonic crystal fibers, IEEE Photon. Technol. Lett. 16 (4) (2004) 1065–1067.
[24] P.S.J. Russell, Photonic-crystal fibers, J. Lightwave Technol. 24 (12) (2006) 4729–4749.
[25] E.K. Akowuah, T. Gorman, H. Ademgil, S. Haxha, G.K. Robinson, J.V. Oliver, Numerical analysis of a photonic crystal fiber for biosensing applications, IEEE J. Quantum Electron. 48 (11) (2012) 1403–1410.
[26] D. Lopez-Torres, C. Elosua, J. Villatoro, J. Zubia, M. Rothhardt, K. Schuster, F. J. Arregui, Photonic crystal fiber interferometer coated with a pah/paa nanolayer as humidity sensor, Sensors Actuators B Chem. 242 (2017) 1065–1072.
[27] J. Wang, B. Liu, Y. Wu, Y. Mao, L. Zhao, T. Sun, T. Nan, Y. Han, Temperature insensitive fiber fabry-perot/mach-zehnder hybrid interferometer based on photonic crystal fiber for transverse load and refractive index measurement, Opt. Fiber Technol. 56 (2020) 102163.
[28] F. Ahmed, S. Roy, B.K. Paul, K. Ahmed, A.N. Bahar, Extremely low loss of photonic crystal fiber for terahertz wave propagation in optical communication applications, J. Opt. Commun. 41 (4) (2020) 393–401.
[29] C. Li, B. Yan, J. Liu, Refractive index sensing characteristics in a d-shaped photonic quasi-crystal fiber sensor based on surface plasmon resonance, JOSA A 36 (10) (2019) 1663–1668.
[30] J.N. Dash, R. Jha, R. Das, Micro-air cavity incorporated tapered-tip photonic crystal fiber based compact refractometer, Laser Phys. Lett. 17 (5) (2020) 055101.
[31] P. Sharma, P. Sharan, Design of photonic crystal-based biosensor for detection of glucose concentration in urine, IEEE Sensors J. 15 (2) (2014) 1035–1042.
[32] A. Rifat, G.A. Mahdiraji, Y. Sua, Y. Shee, R. Ahmed, D.M. Chow, F.M. Adikan, Surface plasmon resonance photonic crystal fiber biosensor: a practical sensing approach, IEEE Photon. Technol. Lett. 27 (15) (2015) 1628–1631.
[33] I.K. Yakasai, P.E. Abas, H. Suhaimi, F. Begum, Low loss and highly birefringent photonic crystal fibre for terahertz applications, Optik 206 (2020) 164321.
[34] M.B. Hossain, E. Podder, Design and investigation of pcf-based blood components sensor in terahertz regime, Appl. Phys. A 125 (12) (2019) 1–8.
[35] V. Kaur, S. Singh, Design approach of solid-core photonic crystal fiber sensor with sensing ring for blood component detection, J. Nanophoton. 13 (2) (2019) 026011.
[36] K. Mileńko, D.J.J. Hu, P.P. Shum, T. Zhang, J.L. Lim, Y. Wang, T.R. Woliński, H. Wei, W. Tong, Photonic crystal fiber tip interferometer for refractive index sensing, Opt. Lett. 37 (8) (2012) 1373–1375.
[37] C.J. Strachan, P.F. Taday, D.A. Newnham, K.C. Gordon, J.A. Zeitler, M. Pepper, T. Rades, Using terahertz pulsed spectroscopy to quantify pharmaceutical polymorphism and crystallinity, J. Pharm. Sci. 94 (4) (2005) 837–846.
[38] T.S. Saini, A. Kumar, Y. Kalra, R.K. Sinha, et al., Rectangular-core large-mode-area photonic crystal fiber for high power applications: design and analysis, Appl. Opt. 55 (15) (2016) 4095–4100.
[39] M. Morshed, M.I. Hassan, T.K. Roy, M.S. Uddin, S.A. Razzak, Microstructure core photonic crystal fiber for gas sensing applications, Appl. Opt. 54 (29) (2015) 8637–8643.

[40] Y. Guo, J. Li, S. Li, Y. Liu, X. Meng, W. Bi, H. Lu, T. Cheng, R. Hao, Amphibious sensor of temperature and refractive index based on d-shaped photonic crystal fibre filled with liquid crystal, Liq. Cryst. 47 (6) (2020) 882–894.
[41] K. Ahmed, F. Ahmed, S. Roy, B.K. Paul, M.N. Aktar, D. Vigneswaran, M.S. Islam, Refractive index-based blood components sensing in terahertz spectrum, IEEE Sensors J. 19 (9) (2019) 3368–3375.
[42] J. Folkenberg, M. Nielsen, N. Mortensen, C. Jakobsen, H. Simonsen, Polarization maintaining large mode area photonic crystal fiber, Opt. Express 12 (5) (2004) 956–960.
[43] M.-Y. Chen, Polarization-maintaining large-mode-area photonic crystal fibres with solid microstructured cores, J. Opt. A Pure Appl. Opt. 9 (10) (2007) 868.
[44] J. Sultana, M.S. Islam, M. Faisal, M.R. Islam, B.W.-H. Ng, H. Ebendorff-Heidepriem, D. Abbott, Highly birefringent elliptical core photonic crystal fiber for terahertz application, Opt. Commun. 407 (2018) 92–96.
[45] E. Podder, M.B. Hossain, R.H. Jibon, A.A.-M. Bulbul, H.S. Mondal, Chemical sensing through photonic crystal fiber: sulfuric acid detection, Front. Optoelectron. 12 (4) (2019) 372–381.
[46] V. Kaur, S. Singh, A dual-channel surface plasmon resonance biosensor based on a photonic crystal fiber for multianalyte sensing, J. Comput. Electron. 18 (1) (2019) 319–328.
[47] M.B. Hossain, E. Podder, A.A.-M. Bulbul, H.S. Mondal, Bane chemicals detection through photonic crystal fiber in thz regime, Opt. Fiber Technol. 54 (2020) 102102.
[48] S. Roy, Fiber optic sensor for determining adulteration of petrol and diesel by kerosene, Sensors Actuators B Chem. 55 (2–3) (1999) 212–216.
[49] A. Pathak, R. Gangwar, P. Priyadarshini, V. Singh, A robust optical fiber sensor for the detection of petrol adulteration, Optik 149 (2017) 43–48.
[50] M.S. Hossain, S. Sen, Design and performance improvement of optical chemical sensor based photonic crystal fiber (pcf) in the terahertz (thz) wave propagation, Silicon (2020) 1–9.
[51] H. Ademgil, Highly sensitive octagonal photonic crystal fiber based sensor, Optik 125 (20) (2014) 6274–6278.
[52] M. Abdullah-Al-Shafi, S. Sen, Design and analysis of a chemical sensing octagonal photonic crystal fiber (o-pcf) based optical sensor with high relative sensitivity for terahertz (thz) regime, Sens. Bio-Sens. Res. 29 (2020) 100372.
[53] S.A. Razzak, Y. Namihira, M.A.G. Khan, F. Begum, S. Kaijage, Guiding properties of a decagonal photonic crystal fiber, J. Microwaves, Optoelect. Electromag. Appl. 6 (1) (2007) 44–49.
[54] K. Ahmed, M. Morshed, S. Asaduzzaman, M.F.H. Arif, Optimization and enhancement of liquid analyte sensing performance based on square-cored octagonal photonic crystal fiber, Optik 131 (2017) 687–696.
[55] R. Hao, Z. Li, G. Sun, L. Niu, Y. Sun, Analysis on photonic crystal fibers with circular air holes in elliptical configuration, Opt. Fiber Technol. 19 (5) (2013) 363–368.
[56] V. Kaur, S. Singh, Extremely sensitive multiple sensing ring pcf sensor for lower indexed chemical detection, Sens. Bio-Sens. Res. 15 (2017) 12–16.
[57] Y. Hou, F. Fan, Z.-W. Jiang, X.-H. Wang, S.-J. Chang, Highly birefringent polymer terahertz fiber with honeycomb cladding, Optik-Int. J. Light Elect. Optics 124 (17) (2013) 3095–3098.
[58] S. Asaduzzaman, K. Ahmed, T. Bhuiyan, T. Farah, Hybrid photonic crystal fiber in chemical sensing, SpringerPlus 5 (1) (2016) 1–11.
[59] K. Ahmed, M. Morshed, Design and numerical analysis of microstructured-core octagonal photonic crystal fiber for sensing applications, Sens. Bio-Sens. Res. 7 (2016) 1–6.
[60] F. Iqbal, S. Biswas, A.A.-M. Bulbul, H. Rahaman, M.B. Hossain, M.E. Rahaman, M. A. Awal, Alcohol sensing and classification using pcf-based sensor, Sens. Bio-Sens. Res. 30 (2020) 100384.
[61] S. Sen, M. Abdullah-Al-Shafi, A.S. Sikder, M.S. Hossain, M.M. Azad, Zeonex based decagonal photonic crystal fiber (d-pcf) in the terahertz (thz) band for chemical sensing applications, Sens. Bio-Sens. Res. 31 (2021) 100393.
[62] A. Habib, A.N.Z. Rashed, H.M. El-Hageen, A.M. Alatwi, Extremely sensitive photonic crystal fiber–based cancer cell detector in the terahertz regime, Plasmonics (2021) 1–10.
[63] A.M. Maidi, I. Yakasai, P.E. Abas, M.M. Nauman, R.A. Apong, S. Kaijage, F. Begum, Design and simulation of photonic crystal fiber for liquid sensing, in: Photonics vol. 8, Multidisciplinary Digital Publishing Institute, 2021, p. 16.
[64] M.J.B.M. Leon, S. Abedin, M.A. Kabir, A photonic crystal fiber for liquid sensing application with high sensitivity, birefringence and low confinement loss, Sensors Int. 2 (2021) 100061.
[65] J. Sultana, M.R. Islam, M. Faisal, K.M.A. Talha, M.S. Islam, Design and analysis of a zeonex based diamond-shaped core kagome lattice photonic crystal fiber for t-ray wave transmission, Opt. Fiber Technol. 47 (2019) 55–60.
[66] B.K. Paul, K. Ahmed, Highly birefringent Topas based single mode photonic crystal fiber with ultra-low material loss for terahertz applications, Opt. Fiber Technol. 53 (2019) 102031.
[67] M. Goto, A. Quema, H. Takahashi, S. Ono, N. Sarukura, Teflon photonic crystal fiber as terahertz waveguide, Jpn. J. Appl. Phys. 43 (2B) (2004) L317.
[68] S. Hossain, A. Mollah, K. Hosain, I.M. Ankan, Thz spectroscopic sensing of liquid chemicals using hollow-core anti-resonant fiber, OSA Continuum 4 (2) (2021) 621–632.
[69] B. Morova, N. Bavili, O. Yaman, B. Yigit, M. Zeybel, M. Aydın, B. Dogan, R. Kasztelanic, D. Pysz, R. Buczynski, et al., Fabrication and characterization of large numerical aperture, high-resolution optical fiber bundles based on high-contrast pairs of soft glasses for fluorescence imaging, Opt. Express 27 (7) (2019) 9502–9515.
[70] S. Ertman, T.R. Wolinski, D. Pysz, R. Buczynski, E. Nowinowski-Kruszelnicki, R. Dabrowski, Low-loss propagation and continuously tunable birefringence in high-index photonic crystal fibers filled with nematic liquid crystals, Opt. Express 17 (21) (2009) 19298–19310.
[71] M.R.H. Khan, A.A. Chowdhury, M.R. Islam, M.S. Hosen, M.H. Mim, M.M. Nishat, Wave-shaped microstructure cancer detection sensor in terahertz band: design and analysis, Appl. Sci. 13 (9) (2023) 5784.
[72] M.R.H. Khan, F.A.M. Ali, M.R. Islam, Thz sensing of covid-19 disinfecting products using photonic crystal fiber, Sens. Bio-Sens. Res. 33 (2021) 100447.
[73] S. Sen, K. Ahmed, Design of terahertz spectroscopy based optical sensor for chemical detection, SN Appl. Sci. 1 (10) (2019) 1215.
[74] S. Sen, S. Chowdhury, K. Ahmed, S. Asaduzzaman, Design of a porous cored hexagonal photonic crystal fiber based optical sensor with high relative sensitivity for lower operating wavelength, Photon. Sens. 7 (2017) 55–65.
[75] M.I. Islam, K. Ahmed, S. Sen, S. Chowdhury, B.K. Paul, M.S. Islam, M.B.A. Miah, S. Asaduzzaman, Design and optimization of photonic crystal fiber based sensor for gas condensate and air pollution monitoring, Photon. Sens. 7 (2017) 234–245.
[76] K. Ahmed, S. Chowdhury, B.K. Paul, M.S. Islam, S. Sen, M.I. Islam, S. Asaduzzaman, Ultrahigh birefringence, ultralow material loss porous core single-mode fiber for terahertz wave guidance, Appl. Opt. 56 (12) (2017) 3477–3483.
[77] M.S. Islam, J. Sultana, A.A. Rifat, A. Dinovitser, B.W.-H. Ng, D. Abbott, Terahertz sensing in a hollow core photonic crystal fiber, IEEE Sensors J. 18 (10) (2018) 4073–4080.
[78] H. Ademgil, S. Haxha, Pcf based sensor with high sensitivity, high birefringence and low confinement losses for liquid analyte sensing applications, Sensors 15 (12) (2015) 31833–31842.
[79] B.K. Paul, M.S. Islam, K. Ahmed, S. Asaduzzaman, Alcohol sensing over o+ e+ s+ c+ l+ u transmission band based on porous cored octagonal photonic crystal fiber, Photon. Sens. 7 (2) (2017) 123–130.
[80] K. Ahmed, S.H. Abdelamir, Development of biological processes for the removal of iron from water intended for the production of drinking water-case of ferruginous waters in Algeria, Int. J. Hydrol. Sci. Technol. 13 (4) (2022) 457–465.
[81] M.M. Hasan, S. Sen, M.J. Rana, B.K. Paul, M.A. Habib, G.M. Daiyan, K. Ahmed, Heptagonal photonic crystal fiber based chemical sensor in thz regime, in: 2019 Joint 8th International Conference on Informatics, Electronics Vision (ICIEV) and 2019 3rd International Conference on Imaging, Vision Pattern Recognition (icIVPR), 2019, pp. 40–44, https://doi.org/10.1109/ICIEV.2019.8858555.
[82] R. Kanmani, K. Ahmed, S. Roy, F. Ahmed, B.K. Paul, M.M. Rajan, The performance of hosting and core materials for slotted core q-pcf in terahertz spectrum, Optik 194 (2019) 163084.
[83] M.S. Islam, J. Sultana, K. Ahmed, M.R. Islam, A. Dinovitser, B.W.-H. Ng, D. Abbott, A novel approach for spectroscopic chemical identification using photonic crystal fiber in the terahertz regime, IEEE Sensors J. 18 (2) (2018) 575–582, https://doi.org/10.1109/JSEN.2017.2775642.
[84] R.H. Jibon, M.E. Rahaman, M.A. Alahe, Detection of primary chemical analytes in the thz regime with photonic crystal fiber, Sens. Bio-Sens. Res. 33 (2021) 100427.
[85] H. El Hamzaoui, Y. Ouerdane, L. Bigot, G. Bouwmans, B. Capoen, A. Boukenter, S. Girard, M. Bouazaoui, Sol-gel derived ionic copper-doped microstructured optical fiber: a potential selective ultraviolet radiation dosimeter, Opt. Express 20 (28) (2012) 29751–29760.
[86] B. Dabas, R. Sinha, Dispersion characteristic of hexagonal and square lattice chalcogenide as2se3 glass photonic crystal fiber, Opt. Commun. 283 (7) (2010) 1331–1337.
[87] V.R.K. Kumar, A. George, W. Reeves, J. Knight, P.S.J. Russell, F. Omenetto, A. Taylor, Extruded soft glass photonic crystal fiber for ultrabroad supercontinuum generation, Opt. Express 10 (25) (2002) 1520–1525.
[88] M. El-Amraoui, G. Gadret, J. Jules, J. Fatome, C. Fortier, F. Désévédavy, I. Skripatchev, Y. Messaddeq, J. Troles, L. Brilland, et al., Microstructured chalcogenide optical fibers from as 2 s 3 glass: towards new ir broadband sources, Opt. Express 18 (25) (2010) 26655–26665.
[89] W. Talataisong, R. Ismaeel, S.R. Sandoghchi, T. Rutirawut, G. Topley, M. Beresna, G. Brambilla, Novel method for manufacturing optical fiber: extrusion and drawing of microstructured polymer optical fibers from a 3d printer, Opt. Express 26 (24) (2018) 32007–32013.
[90] Z. Liu, H.-Y. Tam, Fabrication and sensing applications of special microstructured optical fibers, in: F. Xu, C. Mou (Eds.), Selected Topics on Optical Fiber Technologies and Applications, 2017, pp. 1–20.
[91] D. Pysz, I. Kujawa, R. Stepień, M. Klimczak, A. Filipkowski, M. Franczyk, L. Kociszewski, J. Buźniak, K. Haraśny, R. Buczyński, Stack and draw fabrication of soft glass microstructured fiber optics, Bull. Polish Acad. Sci. Tech. Sci. 62 (4).
[92] A.L. Cruz, C. Cordeiro, M.A. Franco, 3d printed hollow-core terahertz fibers, Fibers 6 (3) (2018) 43.
[93] K. Ahmed, M.I. Islam, S. Sen, B.K. Paul, M.S. Islam, S. Chowdhury, M.R. Hasan, M. S. Uddin, S. Asaduzzaman, A.N. Bahar, Low-loss single mode terahertz microstructure fiber with near-zero-flattened dispersion, Adv. Sci. Eng. Med. 9 (10) (2017) 829–836.
[94] S. Atakaramians, S. Afshar, H. Ebendorff-Heidepriem, M. Nagel, B.M. Fischer, D. Abbott, T.M. Monro, Thz porous fibers: design, fabrication and experimental characterization, Opt. Express 17 (16) (2009) 14053–14062.
[95] D. Pysz, R. Stepien, I. Kujawa, R. Kasztelanic, T. Martynkien, F. Berghmans, H. Thienpont, R. Buczynski, Development of silicate hollow core photonic crystal fiber, Photon. Lett. Poland 2 (1) (2010) 7–9.
[96] A.V. Mitrofanov, Y.M. Linik, R. Buczynski, D. Pysz, D. Lorenc, I. Bugar, A. A. Ivanov, M.V. Alfimov, A.B. Fedotov, A.M. Zheltikov, Highly birefringent silicate glass photonic-crystal fiber with polarization-controlled frequency-shifted

output: a promising fiber light source for nonlinear raman microspectroscopy, Opt. Express 14 (22) (2006) 10645–10651.
[97] P. Russell, Photonic crystal fibers, Science 299 (5605) (2003) 358–362.
[98] M.R. Islam, A. Iftekher, F. Noor, M.R.H. Khan, M. Reza, M.M. Nishat, et al., Azo-coated plasmonic pcf nanosensor for blood constituent detection in near-infrared and visible spectrum, Appl. Phys. A 128 (1) (2022) 1–13.
[99] E. Sokullu, Z.L. Cücük, M.R. Sarabi, M.T. Birtek, H.S. Bagheri, S. Tasoglu, Microfluidic invasion chemotaxis platform for 3d neurovascular co-culture, Fluids 7 (7) (2022) 238.
[100] M. Rezapour Sarabi, S.A. Nakhjavani, S. Tasoglu, 3d-printed microneedles for point-of-care biosensing applications, Micromachines 13 (7) (2022) 1099.
[101] V. Portosi, D. Laneve, M.C. Falconi, F. Prudenzano, Advances on photonic crystal fiber sensors and applications, Sensors 19 (8) (2019) 1892.
[102] J.F. Algorri, D.C. Zografopoulos, A. Tapetado, D. Poudereux, J.M. Sánchez-Pena, Infiltrated photonic crystal fibers for sensing applications, Sensors 18 (12) (2018) 4263.